Interdomain communication in the phosphatidylcholine regulatory enzyme, CCTα, relies on a modular αE helix

Received for publication, June 18, 2019, and in revised form, August 18, 2019 Published, Papers in Press, September 4, 2019, DOI 10.1074/jbc.RA119.009849

Svetla G. Taneva[‡], Jaeyong Lee[‡], Daniel G. Knowles[‡1], Chanajai Tishyadhigama[‡2], Hongwen Chen[§], and Rosemary B. Cornell[‡§3]

From the Departments of [‡]Molecular Biology and Biochemistry and [§]Chemistry, Simon Fraser University, Burnaby, British Columbia V5A 1S6, Canada

Edited by George M. Carman

CTP:phosphocholine cytidylyltransferase (CCT), the rate-limiting enzyme in phosphatidylcholine (PC) synthesis, is an amphitropic enzyme that regulates PC homeostasis. Recent work has suggested that CCTα activation by binding to a PC-deficient membrane involves conformational transitions in a helix pair (αE) that, along with a short linker of unknown structure (J segment), bridges the catalytic domains of the CCTα dimer to the membrane-binding (M) domains. In the soluble, inactive form, the αE helices are constrained into unbroken helices by contacts with two auto-inhibitory (AI) helices from domain M. In the active, membrane-bound form, the AI helices are displaced and engage the membrane. Molecular dynamics simulations have suggested that AI displacement is associated with hinge-like bending in the middle of the αE, positioning its C terminus closer to the active site. Here, we show that CCTα activation by membrane binding is sensitive to mutations in the αE and J segments, especially within or proximal to the αE hinge. Substituting Tyr-213 within this hinge with smaller uncharged amino acids that could destabilize interactions between the αE helices increased both constitutive and lipid-dependent activities, supporting a link between αE helix bending and stimulation of CCT activity. The solvent accessibilities of Tyr-213 and Tyr-216 suggested that these tyrosines move to new partially buried environments upon membrane binding of CCT, consistent with a folded αE/J structure. These data suggest that signal transduction through the modular αE helix pair relies on shifts in its conformational ensemble that are controlled by the AI helices and their displacement upon membrane binding.

The lipid composition of cell membranes must be regulated to maintain fluidity, elasticity, curvature, surface charge, impermeability, and the optimal function of both integral and peripheral membrane proteins that depend on these physical properties. The major membrane phospholipid component in most eukaryotic cells is phosphatidylcholine (PC).[4] The geometrical and packing properties of PC molecules impart strong barrier functions and low curvature strain. In addition to its membrane structural role, PC is a major component of lung surfactant, serum lipoproteins, and bile.

PC homeostasis is controlled in part by the activity of the rate-limiting enzyme in the CDP-choline pathway, CTP:phosphocholine cytidylyltransferase (CCT) (1). CCTs catalyze the synthesis of CDP-choline from CTP and phosphocholine. CCTα is the dominant isoform, and CCTβ is tissue-restricted. Whereas their disordered termini are divergent, their catalytic and membrane-binding domains are >98% similar within a species (1). CCTα, hereafter referred to as simply CCT, is the most intensely studied form. It is activated by translocation to membrane sites that have reduced PC content, according to the prevailing theory. When unbound to membranes *in vitro*, the CCT catalytic efficiency is reduced by more than 2 orders of magnitude by effects on both k_{cat} and the K_m for CTP (2, 3). It is the physical properties of the PC-depleted membrane that attract CCT, properties such as high surface charge and packing voids that accompany a bilayer relatively enriched in acidic and/or nonbilayer-forming lipids (4). Once CCT is membrane-bound and activated, PC production will ramp up and the membrane PC content will be restored, with ensuing release of CCT. As testament to its importance in the supply of PC, three human inherited diseases are caused by single nucleotide changes in PCYT1A, the gene for the CCTα isoform. The mutations destabilize and/or inactivate the enzyme (5) and manifest as dystrophy in retina, bone and cartilage, or adipose tissue (6–9). The question we are trying to solve is: How does membrane binding activate this enzyme?

CCTs are homodimers with each monomer composed of an N-terminal catalytic domain (domain C) and a C-terminal regulatory domain. The latter contains a membrane-binding domain (M) of ~70 amino acids and a C-terminal phosphorylation region (P) of ~50 amino acids. The M domain of CCT has two conformations. Engagement with membranes is accompa-

This work was supported by a grant from the Canadian Institutes for Health Research (to R. B. C.). The authors declare that they have no conflicts of interest with the contents of this article.
This article contains Table S1 and Figs. S1–S7.

[1] Present address: Animal Health Branch, British Columbia Ministry of Agriculture, Abbotsford, British Columbia V3G 2M3, Canada.
[2] Present address: Faculty of Health Sciences, Simon Fraser University, Burnaby, British Columbia V5A 1S6, Canada.
[3] To whom correspondence may be addressed: Dept. of Molecular Biology and Biochemistry, Simon Fraser University, Burnaby, British Columbia V5A 1S6, Canada. Tel.: 778-782-3709; E-mail: cornell@sfu.ca.

[4] The abbreviations used are: PC, phosphatidylcholine; CCT, CTP:phosphocholine cytidylyltransferase; GCT, CTP:glycerolphosphate cytidylyltransferase; ECT, CTP:ethanolaminephosphate cytidylyltransferase; AI, auto-inhibitory; domains C, M, and P, catalytic, membrane-binding, and phosphorylation domains, respectively; POPC, 1-palmitoyl-2-oleoyl-*sn*-glycero-3-phosphocholine; PG, phosphatidylglycerol; PDB, Protein Data Bank; T_m, temperature at the midpoint of unfolding; SLV, sucrose-loaded vesicle; Ni-NTA, nickel-nitrilotriacetic acid.

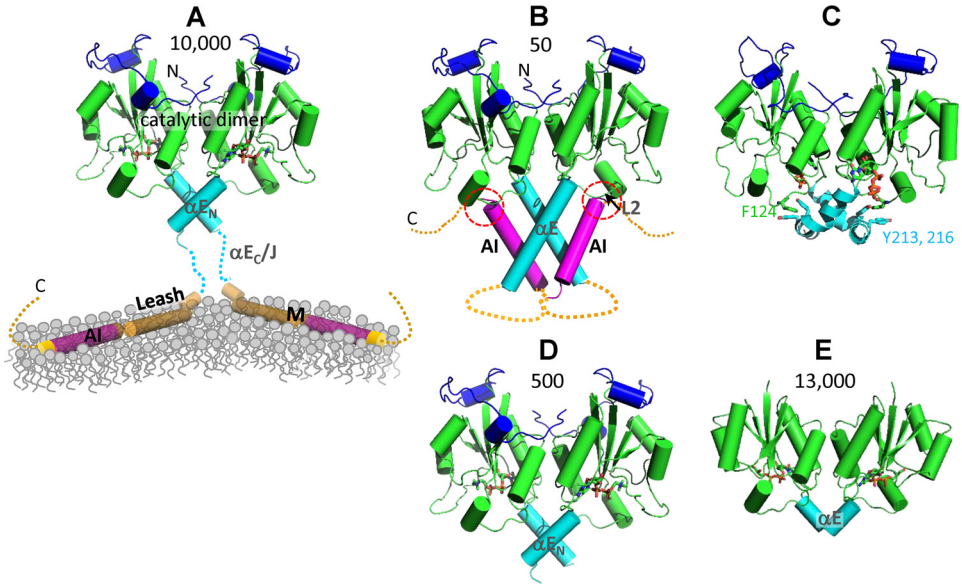

Figure 1. Comparison of the structures of CTs with differing activities. The approximate k_{cat}/K_m values in M^{-1} s^{-1} for each CT form are provided *above* each structure. *A*, CCT_{mem}. This image is a proposed structure created from an amalgamation of solved structures. The catalytic domain cartoon of residues 40–215/216 with bound CDP-choline (*sticks*) is from PDB entry 3HL4, and the domain M helix is a merge of PDB entries 1PEH and 1PEI. Segments with unknown structures are depicted as *dashed lines* in this and other Fig. 1 images. The N-terminal 40 residues, present in the constructs shown in *A–D*, is disordered and not visible in any of the structures. GCT lacks this disordered region. *B*, CCT_{sol}; residues 40–223 from PDB entry 4MVC. The AI helices (residues 276–295; *magenta*) are docked onto the two αE helices (*cyan*) to create a four-helix complex. The *red circle* highlights the inhibitory interaction between the C terminus of the AI helix and loop L2 housing the catalytic Lys-122. *C*, CCT_{sol} with AI helices removed. From a representative MD simulation with 4MVC as the starting structure, CTP in the active site, and constraints on the $αE_C$ to preserve helical structure (18). The image shown corresponds to the configuration shown in Fig. 5*E* of Ramezanpour *et al.* (18). The αE helix and the aromatic interaction between Tyr-213, Tyr-216, and Phe-124 in loop L2 is *highlighted*. *D*, CCT-236; residues 40–215/216 with bound CDP-choline, from PDB entry 3HL4. *E*, GCT; residues 1–126 with bound CDP-glycerol from PDB entry 1N1D. GCT lacks the N-cap (*dark blue*) found in CCT, has a short loop L5, and, relevant to our discussion, has a shortened αE helix resolved to Ile-126 that is analogous to Ile-209 in rat CCTα.

nied by the folding of >60 residues into a long amphipathic helix (Fig. 1*A*), which binds via a combination of electrostatic and hydrophobic interactions (10–12). When unbound to membranes, this domain is composed of an auto-inhibitory (AI) helix (residues 272–293) tethered to the catalytic domain via a disordered "leash" (residues ~236–271) (2, 13, 14). In the crystal structure of an inactive CCT dimer containing the complete catalytic domain and the M domain with a shortened leash, each AI helix docks onto the αE helix pair that extends from the base of the active site (Fig. 1*B*) (15). The two αE helices and two AI helices form a stable four-helix complex that positions the C termini of the AI helices in backbone-to-backbone contact with loop L2 in the active site (Fig. 1*B*). Loop L2 houses a key catalytic residue, Lys-122 (16, 17).

We recently explored potential mechanisms for catalytic silencing by the AI helix. MD simulations of the CCT dimer with and without the AI helices revealed that docking of the AI helices increased the frequency of an electrostatic trap for Lys-122 that captures its amino group, pre-empting contacts with substrates. The AI helices also constrained the dynamics of the αE helices (18). But upon removal of the AI helices *in silico*, the dynamics of the αE helices was dramatically increased. The binding of CCT to membrane vesicles *in vitro*, which displaces the two AI helices, was linked to an increase in the distance between the two αE helices, monitored by cross-linking at a site in the middle of the αE helix. When remodeling of the αE helices was prevented by a constraining disulfide bond, the enzyme, although membrane-bound, was not activated (18). These findings suggest that reorganization of the αE helix pair accompanies membrane binding and is required for full activation of CCT. However, in the absence of a solved structure of membrane-bound CCT, the precise conformation and mechanism of modulation of the αE helices during activation remain unknown.

All eukaryotic CCTs explored thus far are lipid-regulated, including CCTs from unicellular *S. cerevisiae* and *P. falciparum*. These CCTs have a highly conserved sequence corresponding to the 22-residue αE helix seen in the solved mammalian CCT structure obtained from crystals grown in the absence of lipid (PDB code 4MVC). The αE is followed by a turn at Gly-224. This turn was visible in the low-resolution structure of CCT-312 (15). The turn is followed by a structurally unresolved, conserved 10-residue linker to domain M that we refer to as the J (joining) segment (Figs. 1 and 2). In contrast, nonlipid regulated cytidylyltransferases, such as the CTs that use glycerol phosphate or ethanolamine phosphate as cytidyl acceptors (GCT and ECT) have short αE helices that terminate at or before the residue corresponding to Val-210 (Figs. 1*E* and 2). The differences between regulated and constitutive CTs suggest that the αE and J sequence are conserved in CCTs for an important function, such as transducing the membrane-binding event to the activation of the catalytic domain. We refer to the N-terminal αE segment in CCTs (residues 202–211) that resembles the GCT and ECT αE sequences as the $αE_N$ and consider the $αE_N$ to be part of the catalytic domain fold, as it contains residues that contribute to the active site (19–22). We refer to residues 212–215 as the αE hinge (predicted to be helix-breaking) (1, 23) and residues 216–223 as $αE_C$ (see Fig. 2, *diagram*). Within the CCT αE hinge and $αE_C$, two tyrosines (Tyr-213 and Tyr-216; mammalian numbering), two arginines (Arg-219 and

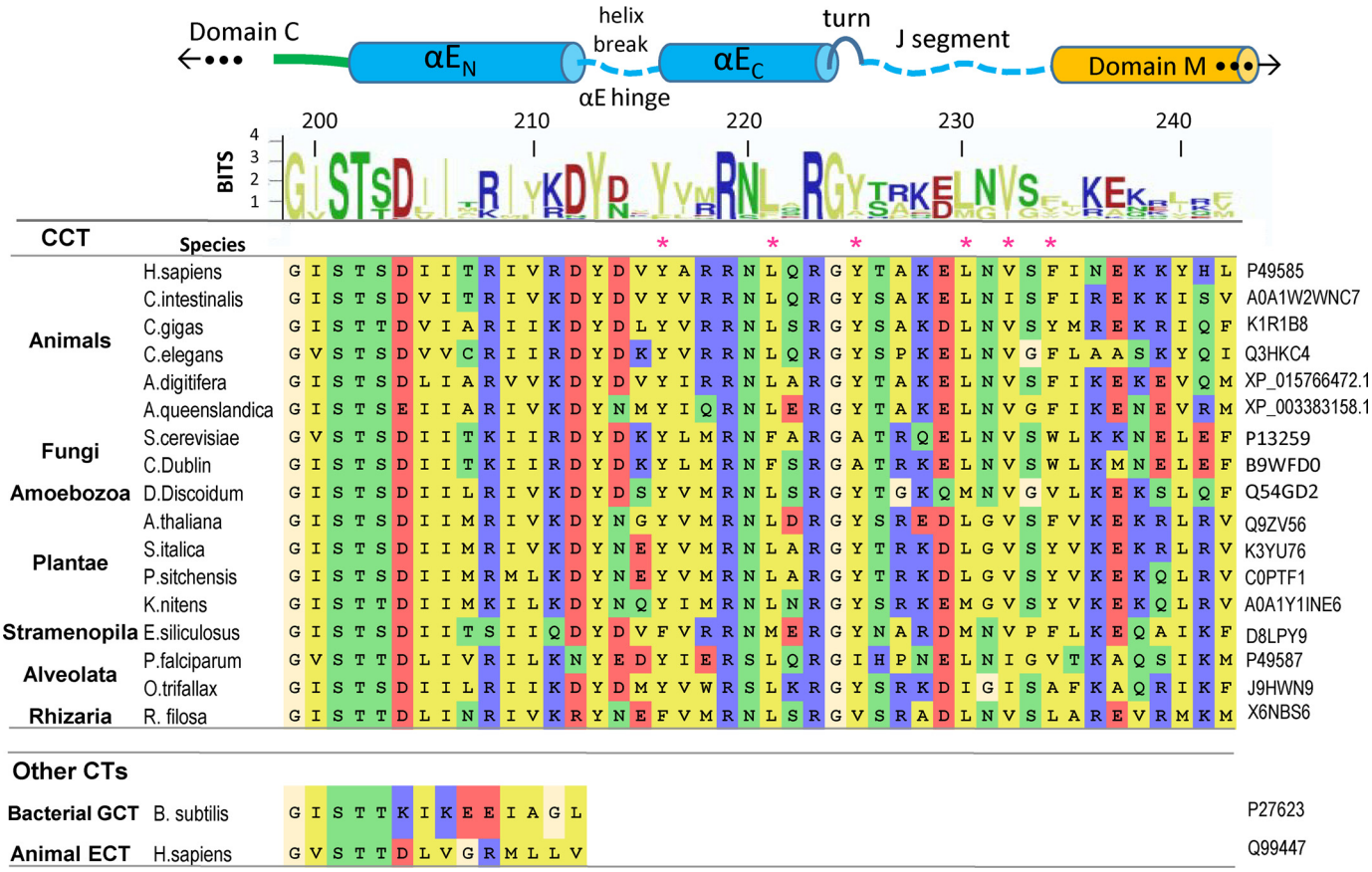

Figure 2. Sequence conservation of αE and J segment. *Top*, *schematic* of the secondary structure of the αE/J segment flanked by domains C and M; rat CCTα numbering. The WEBLogo (http://weblogo.berkeley.edu/logo.cgi) was based on 17 diverse CCT sequences. (Please note that the JBC is not responsible for the long-term archiving and maintenance of this site or any other third party hosted site.) *Middle*, sequence alignment that *color-codes* amino acid conservation. The *asterisks above* the sequence indicate residues in the rat CCTα that were mutated to tryptophan in this study. *Bottom*, the corresponding sequences of the nonlipid-regulated cytidylyltransferases, GCT and ECT (N-terminal repeat), are provided.

Arg-223), and a glycine (Gly-224) appear to be universal. The J segment (residues 225–234) is less strictly conserved, but the sequence conservation is much higher than the M domain.

The previously reported simulations showed that without the constraining AI helices, the two αE helices bent at the predicted break in each of the 10 replicates, and in six of them, the bending led to a new stable conformation featuring splayed helices, each contacting the L2 loops at the base of the active sites, in *trans* (18) (Fig. 1*C*). We hypothesize that a similar conformational change in the αE helices may occur upon membrane engagement via the M domain and that this is required for activation. In this work, we explored this hypothesis by (i) examining the impacts of mutations at conserved sites in the αE on lipid activation and (ii) probing the environment of conserved tyrosines and engineered tryptophans within the αE hinge, αE_C, and J segment in various CCT forms: the soluble form (CCT_{sol}), the membrane-bound form (CCT_{mem}), and a fragment encompassing the catalytic domain and allosteric linker (CCT-236). The catalytic domain and the M and P regions have been extensively probed via mutagenesis. However, the αE and J segments, which constitute the only physical pathway between the membrane-bound M domain and the active site, have never been explored to determine the contribution of conserved sites to catalysis or regulation of catalysis by lipids.

Results

CCT is nonfunctional when truncated to resemble GCT

The k_{cat}/K_m(CTP) value measured for CCT when membrane-bound (9800 s^{-1} M^{-1}; Fig. 3*A*) is similar to that obtained for the constitutively active GCT (13,500 s^{-1} M^{-1}) (20) with its short αE helix. We queried whether a similarly truncated CCT would be constitutively active. However, when we truncated CCT at residue 212 to create a short αE helix like GCT, the enzyme activity was completely obliterated (Fig. 3, *A* and *B*). The transition temperature for unfolding (T_m) for CCT-212, as monitored by Sypro Orange fluorescence, was reduced 10 °C, from 55 °C (full-length) to 45 °C (CCT-212) (Table 1). These data suggest a requirement for some or all of the C-terminal region for CCT catalytic function and catalytic domain stability.

Membrane activation of CCT requires domain M and the J segment

In the absence of membranes the C-terminal region is inhibitory (2, 24, 25). How much of the enzyme C-terminal to domain C contributes to the activation of catalysis in CCT_{mem}? Analysis of CCTs progressively truncated from the C terminus showed that deletion of the P region has little impact on activity (Fig. 3*A*), as noted previously (26–28). But the activity was progressively compromised with increasing truncation of the M domain, especially

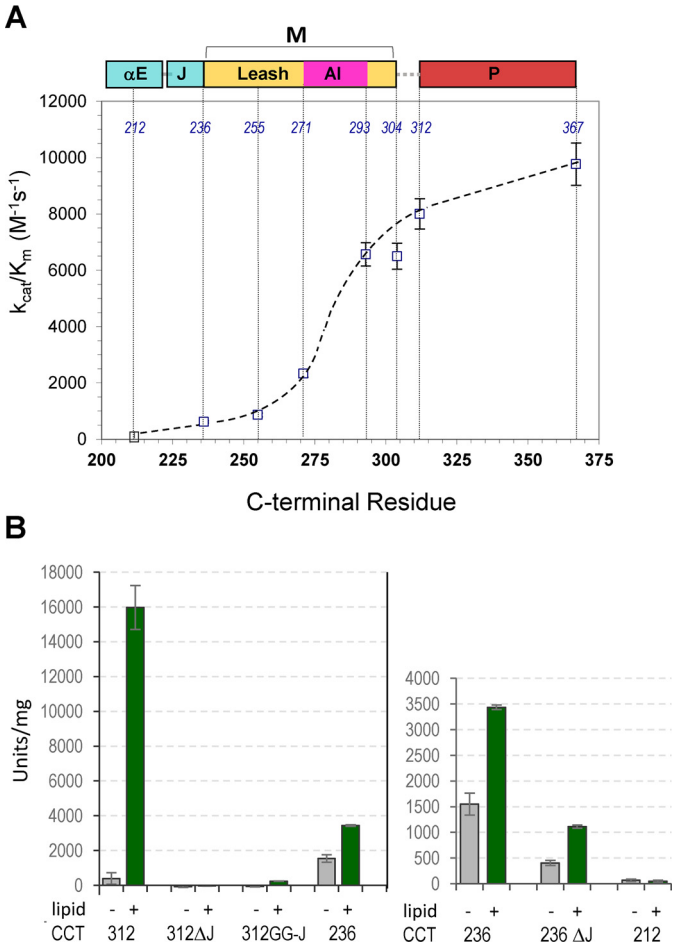

Figure 3. CCT activity relies on the AI segment of domain M, and an intact αE_C and J segment. *A*, constructs truncated at the indicated amino acid were purified, and their k_{cat} and K_m values for CTP were determined in the presence of 0.25 mM PC/PG (1:1) SUVs as described under "Experimental Procedures." *Error bars*, 95% confidence interval. The *dashed line* was added to guide the eye. *B*, the specific activities of the indicated purified CCTs were determined using the standard assay conditions optimal for WT CCT in the absence (*gray*) or presence (*green*) of 0.2 mM PC/PG (1:1) SUVs. One unit is 1 nmol of CDP-choline formed per min. Data are means ± range (*error bars*) of two independent determinations, except $n = 5$ for CCT-312. *GG-J*, replacement with ^{227}GGGSGG^{232}; ΔJ, deletion of residues 227–232.

with loss of the hydrophobic AI helix between residues 272 and 295 (Fig. 3*A*), that contributes strongly to the membrane-binding free energy (2). These decreases are due to impacts on both the k_{cat} and the K_m for CTP (Fig. S1).

Whereas CCT-212 had no measurable activity, ~5% of WT catalytic function is retained with a truncation at the start of domain M (CCT-236; Fig. 3*A*). The truncation at residue 236 did not destabilize the catalytic domain fold, as the T_m for unfolding was equivalent to the full-length enzyme (Table 1). The 10 °C T_m depression measured for CCT-212 indicates that the catalytic domain is adequately stabilized by the αE_C and J segment. The partial constitutive activity of CCT-236 makes sense as it lacks the AI motif. But the low activity of CCT-236 compared with the full-length enzyme in its membrane-bound form also argues that full activation requires domain M to be present and engaged with the membrane.

Following the turn at Gly-224, the J segment comprises 10 conserved amino acids linking the αE_C to the start of domain M. To assess the importance of this sequence to CCT activity, we substituted a glycine-rich J segment, replacing residues 227–232 with GGGSGG, or we simply deleted residues 227–232. Neither of these constructs affected the association of domain M with membrane vesicles as monitored by a lipid fluorescence quenching assay (Fig. S2); nor did they affect the unfolding transition temperature (Table 1). However, both were completely devastating to enzyme V_{max} assayed with or without lipid (Fig. 3*B*). The loss of all activity accompanying the deletion of the J segment is consistent with total inactivation upon truncation at residue 228 (26). Deletion of the 6 residues from the J segment had a milder impact on the activity of CCT-236, lowering it 3-fold (Fig. 3*B*). Thus, both the αE_C and the J segment improve the catalytic function of a CCT missing domain M and are essential for any activity in CCTs with domain M. These data argue that the J segment functions as more than a simple tether between domains.

Conservative site mutations in the αE hinge reduce membrane activation

We analyzed the impact on activity of site-specific mutations at the conserved polar residues in the αE hinge and αE_C segments in the context of CCT-312. This construct contains all of the catalytic and M domains, missing only the P region. This truncation has no negative impact on binding to anionic membrane vesicles *in vitro* (15, 23, 28), as the phosphorylation of this region serves mainly to fine-tune the sensitivity to membrane negative charge (29, 30). A nonconservative replacement of Arg-211 with alanine had no impact on activity with or without lipid vesicles, and conservative substitutions at Tyr-216, Arg-219, Asn-220, and Arg-223 had no effect or a small inhibitory effect (Fig. 4*A*). But several mutations showed activity reductions of >2-fold: D212A, Y213F, and D214A (D214N) in the αE hinge; Y216A at the start of the αE_C; and G224A in the predicted turn at the end of the αE_C. To determine whether these inhibitory effects were selective for membrane-induced activity, we also created the mutations in the context of CCT-236. D212A and especially Y216A and G224A were strongly inactivating in the context of both CCT-236 and CCT-312, suggesting functional roles that are independent of a membrane-bound M domain, but the αE hinge substitutions at Tyr-213 and Asp-214 had minor or negligible consequences on the activity of CCT-236 (Fig. 4*B*). That the hinge mutations required a membrane interaction to manifest a defect suggested that the hinge may be a critical region for signal transduction by membrane binding of domain M.

Destabilizing αE hinge mutations enhance CCT activity

To probe the importance of the αE hinge in membrane activation, we focused on the hinge residue Tyr-213, which shows different interactions in the crystal structures of fully silenced CCT-312 *versus* the partially active CCT-236. In the silenced CCT structure, Tyr-213 is buried in the hydrophobic interior of the four-helix complex and forms a weak H-bond to Asp-214 in *trans* across the dimer interface (Fig. 5*A*). In CCT-236, one of these H-bonding partnerships is intact, but in chain B, a bend at the hinge places the Tyr-213 hydroxyl within H-bonding distance from a backbone carbonyl on loop L2 at

Table 1
T_m for CCT variants
Protein concentration was 2 or 3 μM; Sypro Orange was 5×, diluted from the 5000× concentrate provided by the supplier. "CCT parent" refers to the construct used to engineer the site mutation.

CCT parent	Site mutation	Location of mutation	T_m	*n*
367 untagged	None		55 ± 0.1	2
His-212	None		45 ± 1	2
His-236	None		54 ± 1	3
236 untagged	None		53.5	1
His-236	Y213F	αE hinge	51.0 ± 0.1	2
His-236	Y213T	αE hinge	46.9 ± 0.1	2
His-236	Y213G	αE hinge	47.5 ± 0.5	2
His-236	Y213A	αE hinge	50.5 ± 0.5	2
His-236	Δ227–232	J segment	51.9 ± 0.1	2
His-312	None		57 ± 1	2
His-312	Y213A	αE hinge	49.7 ± 1.2	2
312-His ΔNLS	None		55.5	1
312-His ΔNLS	W151F	Active site	56.0 ± 0.7	3
312-His ΔNLS, W151F	Δ227–232	J segment	57 ± 1	2
312-His ΔNLS, W151F	^{227}GGGSGG^{232}	J segment	57.8 ± 0.25	2
312-His ΔNLS	W278F	AI helix	50	1
312-His ΔNLS, W151F, W278F	Y216W	αE_c helix	51	1
312-His ΔNLS, W151F, W278F	L221W	aEc helix	50	1
312-His ΔNLS, W151F, W278F	L230W	J segment	50.5	1
312-His ΔNLS, W151F, W278F	V232W	J segment	50	1

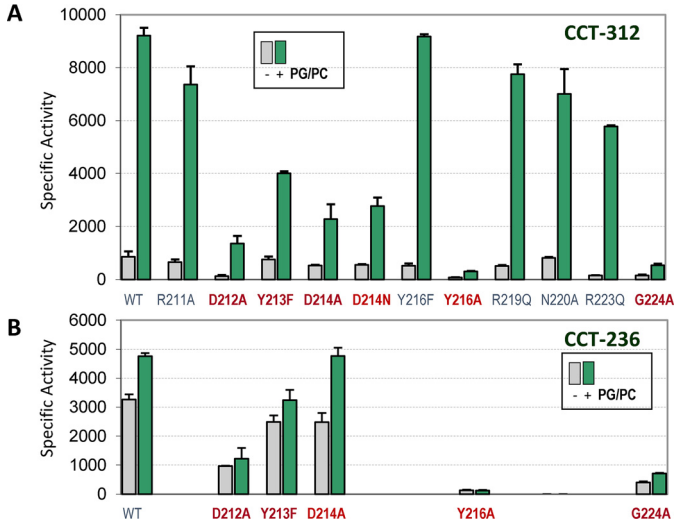

Figure 4. Mutation scan of conserved αE residues identify two αE hinge residues as potential signal transducers between M and C domains. The activities (units/mg of CCT) were determined in the absence (*gray bars*) or presence (*green*) of 0.2 mM PC/PG (1:1) SUVs. The data are means ± S.E. (*error bars*) of 2–4 determinations. *A*, activity of CCT-312 αE/J variants; *B*, activity of CCT-236 αE/J variants.

Phe-124 in chain A (Fig. 5*B*). This is the same carbonyl that participates in the backbone trap for the catalytic lysine (15). In simulations of the catalytic dimer without the AI helices, Tyr-213 is at the center of the αE hinge that samples different configurations on a nanosecond scale (18).

Mutations that replaced Tyr-213 with small aliphatic residues (Thr, Ala, and Gly) destabilized the soluble, silenced form, leading to an increase in the k_{cat}/K_m in the absence of lipid vesicles. This effect was seen in the context of CCT-312, which contains the M domain, and, somewhat surprisingly, CCT-236, which does not (Fig. 5*C*). Thus, the effect of these hinge mutations on activity can be independent of the four-helix complex. These data suggest that weakening of the interactions between the two αE helices may facilitate CCT catalysis. In contrast, tyrosine or phenylalanine at position 213 maintains low activity in the lipid-free state, suggesting that these bulky groups stabilize αE helix interactions and/or the four-helix complex in CCT-312. In keeping with a destabilizing role of the small aliphatic substitutions at Tyr-213, we found that the unfolding transitions of CCT-236 bearing Ala, Thr, or Gly at residue 213 were reduced 4–7 °C, and the T_m for CCT-312(Y213A) was also reduced 7 °C (Table 1). A Phe substitution in the AI helix at Trp-278, a residue vital for maintaining a web of interactions at the base of the four-helix complex (15), also lowered the T_m by 7 °C (Table 1; W278F). Fig. 5*D* shows the packing gap that is created between αE helices when Tyr-213 is changed to alanine.

The activity of CCT-236 is elevated ≤2-fold by lipids, and in the presence of lipid vesicles, the small aliphatic substitutions at Tyr-213 also stimulated activity. For membrane-bound CCT-312, the small aliphatic substitutions were activating compared with a hydrophobic phenylalanine substitution. However, none of the substitutions could mimic the role of tyrosine in the activation of CCT-312 by lipids. Neither the Y213F nor Y213A hinge mutation affected CCT-312 binding to anionic lipid vesicles (Fig. S3); thus, the effects were due to a block in signaling from the membrane-bound M domain. The data of Fig. 5*C* suggest that one role for membrane binding of domain M is to impart activating properties to Tyr-213. These data suggest that Tyr-213 evolved as the solution to effective silencing and activating functions and thus is tuned for regulation by lipids.

Tyr-213 resides in different chemical environments in the inactive, partially active, and fully active forms

MD simulations of residues 40–223 revealed that removal of the AI helices lifted the constraints on the αE helices, leading to hinge bending and persistent contact between Tyr-213 and Tyr-216 with Phe-124 and Val-126 of loop L2 (18) (Fig. 1*C*). To probe the αE conformational switch *in vitro*, we investigated the environment of Tyr-213 and Tyr-216 in three forms of CCT: the soluble inactive form, the fully activated membrane-bound form, and partially active soluble CCT-236. Based on the solved structures of membrane-free CCT-312 and CCT-236, we expected that Tyr-213 would be very protected from solvent in the absence of lipid as it is buried deep within the four-helix bundle and that it would be

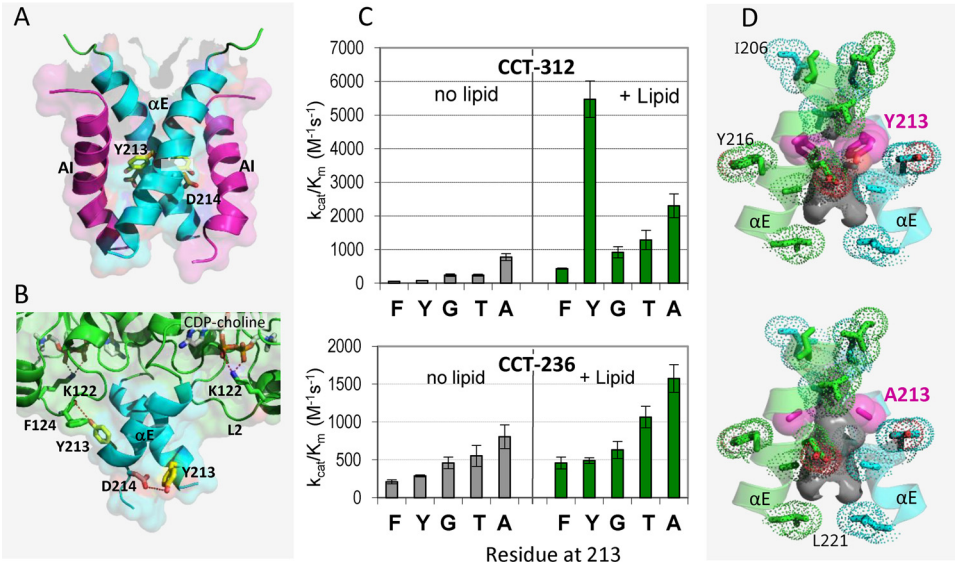

Figure 5. Small aliphatic substitutions for Tyr-213 in the αE hinge promote CCT activity. *A*, disposition of Tyr-213 in CCT_{sol} (PDB entry 4MVC). A *zoom* of the four-helix complex shows the two αE and two AI helices. Tyr-213 and Asp-214 are *highlighted* in *stick representation*. *B*, disposition of Tyr-213 in CCT-236 (PDB entry 3HL4). Shown is a *zoom* of the αE helices and the base of the catalytic domain. A break in the αE on the *left* (chain B) orients Tyr-213 hydroxyl within H-bonding distance of the carbonyl of Phe-124 adjacent to the catalytic residue, Lys-122, which is in contact with CDP-choline. The other Tyr-213 remains directed inward within H-bonding distance of Asp-214 of the other chain. *C*, effect of substitutions for Tyr-213 on constitutive and lipid-dependent activity. To obtain kinetic constants, CCT enzyme activity was assayed as a function of CTP concentration, with fixed phosphocholine concentration (2 mM) in the absence (*gray*) or presence (*green*) of 0.25 mM PC/PG (1:1) SUVs. *Error bars*, 95% confidence interval. *D*, alanine substitution for Tyr-213 creates a packing gap. *Top*, view of the two αE helices in *cyan* and *green* with Tyr-213 in *magenta*; *bottom*, same view with Ala-213 (*magenta spheres*) substituted using the PyMOL mutagenesis function. Hydrophobic side chains lining the αE helix inner face, Asp-214, and Tyr-216 are represented by *dotted spheres*, and the packing gap is portrayed with a *gray space filler*.

more exposed in CCT-236 (Fig. 5, *A* and *B*). How does its exposure in membrane-bound CCT compare with these constructs? We probed the environment of these tyrosines by iodination potential, using chloramine-T–catalyzed iodination of the native enzyme. The iodination was followed by complete trypsin digestion, separation, identification, and quantification of peptides by HPLC and MS. This provided us with information on the accessibility of all 11 tyrosines in the full-length enzyme. Each tyrosine can have 0, 1, or 2 iodo groups, depending on its solvent exposure. This produced a set for each peptide with increasing mass of 126 Da per iodo group (see Figs. S4 and S5 for some examples). The iodination potential correlated well with the accessibility of tyrosines that are buried in the core of the catalytic fold or exposed on a surface loop (Table 2 and Fig. 6*A*). Furthermore, iodination of Tyr-240 in the M domain was reduced 35% in the presence of membranes. These results suggested that our method can provide faithful assessment of the environment of CCT's tyrosines.

The two tyrosines of the αE are housed in a single tryptic peptide corresponding to ^{212}DYDVYAR^{218}; thus, this peptide can contain 0, 1, 2, 3, or 4 iodo groups. These species were separated by HPLC and identified by their masses. Moreover, using a modified LC separation method, we separated the seven positional isomers of this peptide containing 1, 2, or 3 iodo groups, and each unique species was identified by MS/MS fragmentation (Fig. S5).

Iodination of the αE peptide containing Tyr-213 and Tyr-216 was semi-protected compared with tyrosines located on the periphery of the catalytic domain and more exposed than those buried in the hydrophobic core (Table 2). Iodination was enhanced by membrane binding, from 1.44 ± 0.16 iodo groups/peptide in CCT_{sol} to 1.82 ± 0.01 in CCT_{mem}. The average iodination of the peptide was even higher in our analysis of CCT-236, 2.2 ± 0.04 (Fig. 6*B*). Fragmentation analysis of the multiply iodinated peptides (1–3 iodo groups/peptide) provided the iodination status of each tyrosine and the Tyr-213/Tyr-216 iodination ratio (Fig. 6*C*). Tyr-216 iodination was invariant among the three CCT forms (1.06 ± 0.02), whereas Tyr-213 iodination was only 0.4 ± 0.11 iodo groups/peptide in CCT_{sol} and increased to 0.77 ± 0.01 in CCT_{mem}. The ratio of iodination on Tyr-213/Tyr-216 increased from 0.39 ± 0.11 to 0.73 ± 0.01 upon membrane binding, but this ratio is less than that of CCT-236 (1.0 ± 0.04).

These data suggest that displacement of the AI helices that accompanies membrane binding increases the accessibility of Tyr-213, which is not surprising. But the reduced iodination of Tyr-213 of membrane-bound CCT compared with CCT-236 suggests an environment for Tyr-213 in CCT_{mem} that is more sequestered from solvent than in a truncated soluble CCT. The latter is expected to have a disordered αE_C and J segment. Thus, Tyr-213 resides in a semi-protected environment in CCT_{mem}, which is compatible with a folded population for the αE_C in membrane-bound, active CCT.

Membrane binding promotes a new, sequestered environment for residue 216 in the αE

We further probed the environment of the αE hinge and αE_c compared with other segments of CCT by examining the fluorescence of engineered Trp residues and their accessibility to the quencher acrylamide. We engineered Trp substitutions in the αE_C helix and J segment in CCT-312 Trp-free backgrounds (sites shown in Fig. 2 *above* the sequence alignment) and also explored native Trps in the active site (Trp-151) and in the AI segment of domain M (Trp-278). The lipid-stimulated activities of the purified single Trp mutants at Y216W (αE_C), and

Table 2

Iodination status of tyrosines in CCT

CCT_{mem} was prepared by incubating full-length WT CCT with 100-fold molar excess PG SLVs. CCT_{sol} or CCT_{mem} was incubated with oxidized sodium iodide for 2 min using a NaI/Y molar ratio of 3 or a ratio of 2 in the single case of the peptide housing Tyr-133. After complete trypsinolysis, fast-HPLC separation, and MS analysis, the fraction of each peptide sequence with 0, 1, 2, 3, or 4 iodo groups was calculated. The table reports the average number of iodo groups per peptide species. Data are means ± average deviation of two or three independent iodination and MS analyses. Analyses of iodination of these peptides using different iodination ratios of NaI/Y = 1, 2, or 5 provided the same conclusion with regard to whether the tyrosine was exposed or buried. Examples of the distribution of iodinated species are shown in Fig. S4. The values for DYDVYAR peptide in this table are very similar but not identical to the values in Fig. 6 because of the differing separation and analytical methods used here (fast HPLC separation and MS) *versus* Fig. 6 (slow HPLC and MS/MS).

Identity of peptide	Location of Tyr/exposure	Theoretical mass	Measured mass	Iodination CCT_{sol}	Iodination CCT_{mem}
		Da	*Da*		
QPAPFSDEIEVDFSKP^{59}YVR	N-cap/δ exposure	2225.46	2225.36	0.13 ± 0.05	0.5 ± 0.2
V^{80}YADGIFDLFHSGHAR	β1/buried	1805.98	1805.93	0.01	0.08 ± 0.02
NLFPNT^{107}YLIVGVCSDELTHNFK	β2/buried	2525.88	2525.79	Not analyzed	Not analyzed
^{133}YDAVQHCR	αC/buried	992.09	992.05	0.11	0.57 ± 0.01
^{141}YVDEVVR	L3/buried	879.99	879.91	0.00	0.08 ± 0.02
IDFVAHDDIP^{173}YSSAGSDDV^{182}YK	L5/αL/exposed	2315.45	2315.46	3.1 ± 0.1	3.2 ± 0.08
D^{213}YDV^{216}YAR	αE/mixed	901.95	901.95	1.3 ± 0.3	1.91 ± 0.02
G^{225}YTAK	J segment/exposed	539.61	539.34	1.95 ± 0.05	1.91 ± 0.06
Y^{240}HLQER	Domain M/mixed	845.93	845.92	1.95 ± 0.08	1.29 ± 0.05

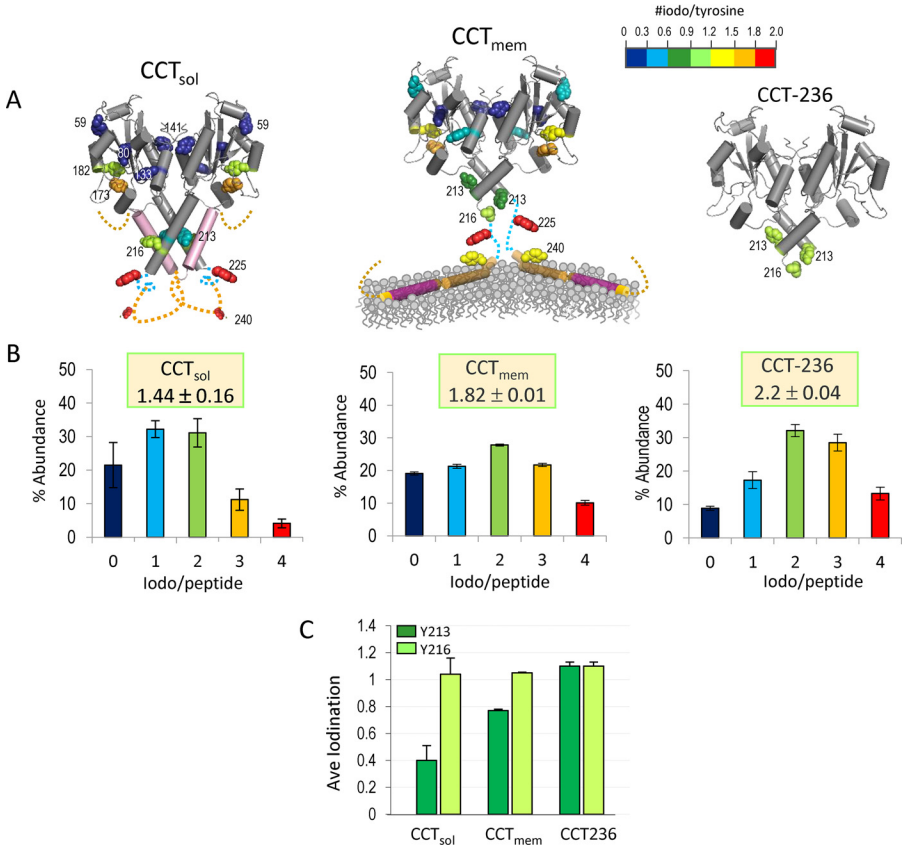

Figure 6. Iodination of Tyr-213 reveals a partially sequestered environment in CCT_{mem}: comparison with CCT_{sol} and CCT236. *A*, *cartoons* depict three forms of CCT with 10 tyrosines shown in *sphere representation* and *color-coded* to reflect the iodination levels reported in Table 2. Tyr-225 and Tyr-240 are not visible in the solved structure of CCT_{sol} or the catalytic fragment, CCT-236; they are placed manually near their expected location on the *cartoon* of CCT_{sol}. Only one Tyr-216 is visible in the solved structure of CCT-236. Analysis of the iodination status for CCT-236 was performed only for the αE peptide. *B*, distribution of iodinated species of the αE peptide, ^{212}DYDVYAR^{223}, containing the indicated number of iodo groups per peptide, assessed by quantitative MS methods. The *values* in the *boxes* indicate the average iodination for the peptide derived from the distribution. *C*, the average iodination levels for Tyr-213 and Tyr-216 are shown for the three CCT forms, calculated from the distributions shown in *B*. The data for *B* and *C* are means ± range (*error bars*) of two independent iodination reactions and MS analyses.

Y225W and F234W (J segment) were similar to WT (Fig. 7*A*), indicating tolerance to substitution from one aromatic residue to another. However, the activities of L221W, L230W, and especially V232W were impaired, indicating intolerance of an aliphatic to aromatic switch in the αE_C and J segments. The T_m for unfolding was not altered for the Y216W, L221W, L230W, or V232W substitutions compared with the parent enzyme (W278F; T_m = 50.5 ± 0.5 °C; Table 1), and the chymotrypsin digestion patterns were also undistinguishable from the control,[5] confirming that the mutations do not destabilize the catalytic domain fold. Thus, we opted to analyze these variants, but

[5] D. G. Knowles, unpublished observation.

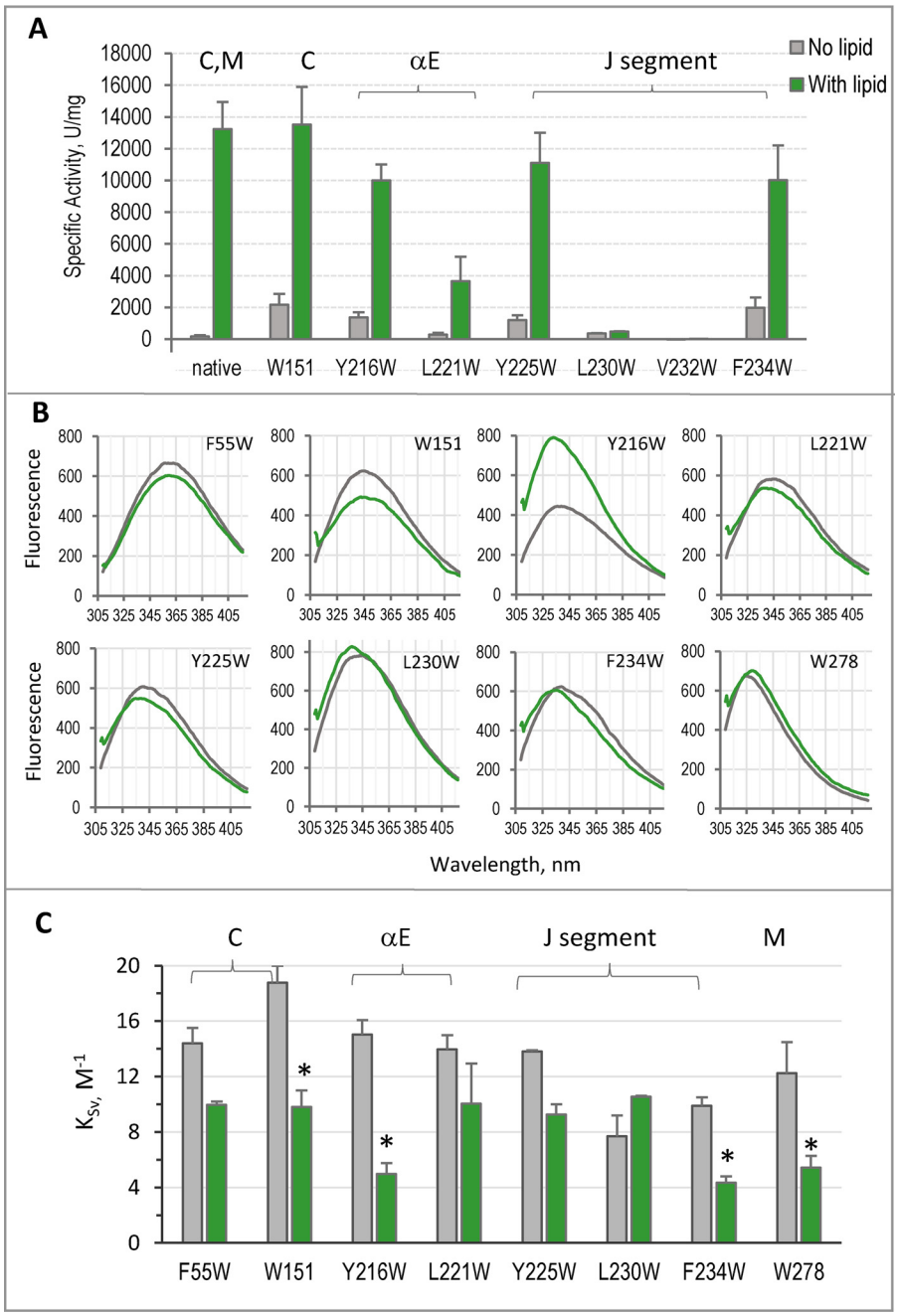

Figure 7. Trp engineering reveals sensitivity of αE_C/J to mutation and large fluorescence changes at the αE hinge. *A*, allosteric linker function is intolerant to nonconservative site mutations. Standard specific activities of native CCT-312 (with native Trps at Trp-151 and Trp-278) and other constructs containing a W278F mutation and one additional engineered Trp at the indicated site. Activity was measured in the absence (*gray*) or presence of 0.2 mM POPC/egg PG (1:1) vesicles (*green*). Data are means ± the range of two independent determinations. *B*, representative fluorescence spectra of single Trp variants in the absence (*gray*) or presence of lipid (*green*). The CCT concentration was 3 μM, and the PC/PG (1:1) vesicle concentration was 450 μM. Spectra are corrected for buffer or lipid background. *C*, acrylamide quenching constants; K_{SV} ± average deviation (*error bars*) of 2–3 independent determinations for the indicated single-Trp mutants in the absence (*gray*) or presence (*green*) of 150-fold molar excess PC/PG (1:1) vesicles. *, $p < 0.05$. Representative spectral sets are provided in Fig. S7.

not the completely inactive V232W. The tryptophans engineered into the αE_C and J segment did not impair the lipid concentration dependence for activation by small anionic lipid vesicles, suggesting no impact on domain M–membrane interaction (Fig. S6).

The fluorescence spectra for these CCTs (Fig. 7*B*) varied in peak wavelength, reflecting the variable environments for each tryptophan. The spectra for Trp-55 in the N-terminal region of domain C was red-shifted (362 nm), reflecting its solvent exposure, and its emission peak was unaffected by lipid vesicles. Trp-278 in the AI helix was highly blue-shifted (326–328 nm) in both CCT_{sol} and CCT_{mem}, reflecting its buried disposition within the four-helix complex and the lipid bilayer, respectively (11, 15, 31, 32). The spectra for Trp-151 in the catalytic domain showed a peak at ~345 nm that was not blue-shifted by lipid vesicles but was reduced in intensity ~20%. The spectra for four

tryptophans in the αE_C/J segment (Trp-221, Trp-225, Trp-230, Trp-234) were moderately blue-shifted in the soluble form (~345 nm), and lipid vesicles caused additional 4–5-nm blue shifts without significant changes in intensity. The spectral behavior of Trp-216 was the most striking. It was solvent-quenched in CCT_{sol} and dramatically dequenched in CCT_{mem}, along with a ~4-nm blue shift, indicating distinct environments for the two states.

Changes in solvent exposure of the single Trps were also assessed by the degree of acrylamide quenching of soluble and membrane-bound forms. Fig. 7*C* shows Stern–Volmer quenching constants (K_{SV}) for the entire set. For comparison, the K_{SV} for Trp amino acid in solution was 25 M^{-1}. All sites showed reduced acrylamide quenching in membrane-bound CCT, with the exception of Trp-230. Membranes offered a high degree of protection for both Trp-234 and Trp-278, lowering the K_{SV} by factors of ~2.5, suggesting that Trp-234 marks the N terminus of domain M. Acrylamide quenching of a Trp engineered into the N-terminal region (F55W) was reduced ~30%, but given the small sample number, this was not statistically significant. The active site Trp-151, however, showed a significant 2-fold reduction in K_{SV}, suggesting a more secluded environment in CCT_{mem}. In soluble CCT, the AI helices should partially protect the nonpolar αE_c residues from solvent; thus, one might anticipate an increase in acrylamide quenching upon membrane binding. However, acrylamide quenching was slightly decreased for Trp-221 and Trp-225 and strongly reduced for Trp-216. Trp-216 showed the strongest membrane protection from acrylamide of all sites, with a 3-fold reduction in K_{SV} (Fig. 7*C*). In CCT_{mem}, the K_{SV} constant for Trp-216 was only 5 ± 0.8, equivalent to those in the M domain, suggesting similar solvent-shielded environments. The combined changes in fluorescence intensity, peak wavelength, and accessibility to solvent indicate a dramatically different environment for Trp-216 in CCT_{sol} *versus* CCT_{mem}.

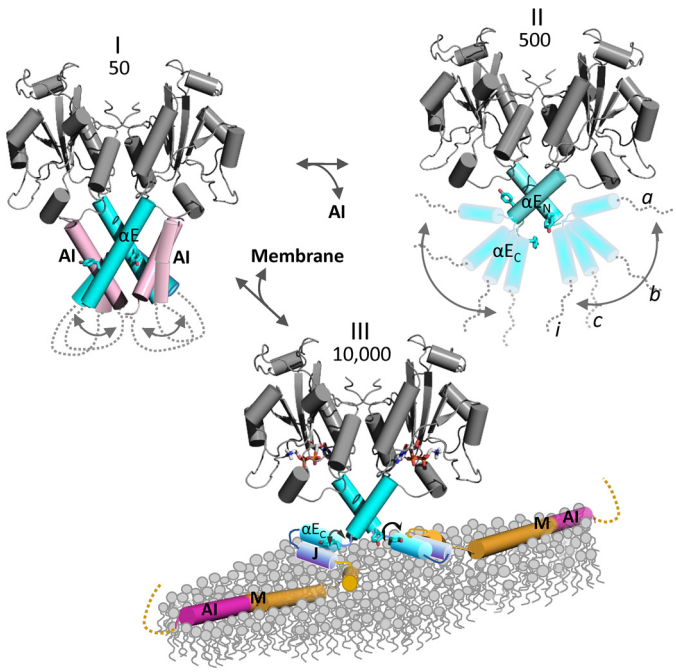

Figure 8. Proposed model: The allosteric linker (hinge, αE_C, J segment) conformational ensemble is modulated by the AI helix and membrane interactions to regulate catalysis. *State I*, CCT_{sol}. The αE makes only modest excursions about its long axis (indicated by *double-headed arrows*), restricted by interactions with the AI helices within a 4-helix complex. The $k_{cat}/K_m \approx 50$ s^{-1} M^{-1}. Image adapted from PDB entry 4MVC. *State II*, *e.g.* CCT-236. Removal of the AI without membrane binding leads to a multitude of ~isoenergetic states for the αE_C, and the configuration most productive for catalysis (*e.g.* conformer *a*) is visited infrequently ($p < 0.1$). This state with a disassembled four-helix complex can also be envisioned as an intermediate to membrane binding. $k_{cat}/K_m \approx 500$ s^{-1} M^{-1}; image from PDB entry 3HL4. The αE_C helices were placed manually. *State III*, CCT_{mem}–M domain embedding in the membrane promotes a folding pathway for the αE_C and J segment, with the lowest energy configuration shown speculatively as a helix-turn-helix following the αE hinge. The configuration of the αE that is most productive for catalysis (conformer *a*) is stabilized by interactions with the J segment and with the membrane surface. *Arrows*, small rotations about the αE hinge. The $k_{cat}/K_m \approx$ 10,000 s^{-1} M^{-1}; image from PDB entries 4MVC (residues 40–216 only), 1PEI, and 1PEH. The αE_C and J segments were placed manually. αE residues Tyr-213 and Tyr-216 are shown in *stick representation* in all three states.

Discussion

This work is the first report of the participation of residues in the αE and J segments in the regulation of catalysis upon membrane binding via domain M. The αE_C and J segments may function together as an allosteric switch. Truncation and deletion mutations in αE_C/J completely obliterated activation of CCT_{mem} by lipids. Even nonconservative single-site mutations in this region caused drastic reductions in enzyme activity, suggesting a role beyond the simple tethering of two domains. The data here also suggest a conformation for the αE_C/J in CCT_{mem} that differs from previous models that portrayed it as an extended, unstructured tether between the catalytic and membrane-bound domains (*e.g.* see Fig. 1). The disposition of the αE_C/J in relation to the catalytic domain and the membrane surface is explored in the companion paper (33). The emerging model presented here (Fig. 8) and bolstered by data in the companion paper proposes that the allosteric function of the αE_c and J segment rely on their metastability. Membrane binding of the M domain provides an anchor to restrict the ensemble of conformers and thereby direct the folding of the allosteric linker into conformations productive for catalysis.

Tyr-213 has a role in both silencing and activation

The mutation scan through the αE directed us to focus on the consequences of mutations at the αE hinge. Two hinge mutations we initially tested had impacts only on CCT with an intact M domain (CCT-312 but not CCT-236), implying hinge involvement in signal transduction from the M domain. A set of substitutions for Tyr-213 provided evidence that this tyrosine has evolved as an effective solution to both silencing and activation of catalysis. In support of a silencing role, constitutive activity was elevated by mutations that change bulky Tyr-213 to smaller residues that destabilized the four-helix complex. In the solved structure (PDB code 4MVC (15)), Tyr-213 contributes to the stability of the inactivating four-helix complex by occupying the center of a hydrophobic pocket bounded by Ala-217 of the same αE, Val-210 of the partnering αE, and Phe-285, Ile-289, and Phe-289 of the AI helix. Tyr-213 can also H-bond in *trans* with Asp-214. That a Phe substitution for Tyr-213 did not elevate the activity of the soluble form argues that the polar contact is a weak one and that hydrophobic packing optimization is the dominant role for Tyr-213 in silencing.

The latter would be disrupted by the small aliphatic substitutions (Fig. 5*D*).

Destabilization of inactive conformers (*e.g.* by membrane displacement of the AI helices or a Y213A mutation) provides the opportunity for generating new activating conformers. Without the docked AI helices, there are very few αE_C protein contacts (see Fig. 5*D*), so that they appear poised for rearrangement. However, if dynamics alone were sufficient for activation, then the glycine substitution should have had the greatest desilencing effect, but glycine was a poorer substitute than Ala or Thr for both CCT_{sol} and CCT_{mem} activity. Thus, whereas hinge dynamics enables the αE_C/J to adopt different environments, constrained hinge movements, limited by the membrane-embedded M domain, reduce the number of nonproductive conformers. We had previously hypothesized an αE-ordering role for membrane binding in the activation of CCT, based on correlations between crystallographic B factors for the αE helix and enzyme activity in various CT structures (19). Our new analysis of mutational effects supports an organizing role for the domain M–membrane interaction.

In support of an activating function for Tyr-213, no substitution was as effective as the native tyrosine for CCT_{mem}. We do not know the precise role of Tyr-213 in catalysis, but the data of Fig. 5*C* suggest that membrane binding empowers its participation (*e.g.* by stabilizing a specific orientation of the Tyr-213 hydroxyl for H-bonding). Because both the crystal structure of CCT-236 and the MD simulations featured an interaction in the bent αE configuration between the Tyr-213 hydroxyl and a carbonyl oxygen at Phe-124 in loop L2, we had hypothesized that the membrane-promoted bending of the hinge could position Tyr-213 to capture one partner of the trap for Lys-122, the carbonyl at Phe-124 (1, 18). In this way, Tyr-213 could participate in the lipid regulation of catalysis. However, that Y213A is partially active is difficult to align with this mechanism. Although its mechanism of action remains to be solved, our data suggest that the aromaticity and/or hydrophobicity of Tyr-213 is important for silencing and activation, and its H-bonding capacity is required for optimal catalytic function.

αEc/J mutations can modulate CCT activity independent of domain M

CCT-236 is considered to be in a "desilenced," lipid-independent state, released from the inhibitory action of the AI helix but unable to fully populate the state required for full activation. But surprisingly CCT-236 is weakly activated by lipids (Figs. 3–5), an effect that will be clarified in the companion paper (33). Thus, it is an imperfect model to use compared with CCT-312 to tease out the specific lipid-related effects from nonlipid-related effects on activity. αE hinge, αE_C, and J segment mutations affected the activity of CCT-236, consistent with a role for this region in allosteric control of catalysis. The catalytic enhancement created by mutations at Tyr-213 that destabilize αE–αE packing indicates that the activity inherent in the truncated CCT is also dependent on a malleable αE_C/J conformational ensemble. However, unlike CCT-312, the activation of CCT-236 by lipids was *less* effective with the native tyrosine at position 213 than with alanine. One explanation for these results is that only when the M domain is membrane-bound can a hinge conformation be promoted that positions the Tyr-213 hydroxyl to participate (indirectly) in the reaction.

A guided conformational ensemble model elucidates the impacts of αE hinge mutations

Collectively, these results suggest a model where the allosteric linker samples multiple conformers when the AI is removed, but not all conformers are productive for catalysis (Fig. 8). In CCT-236, the conformation of the αE_C/J that is optimal for full activation of the enzyme (hypothetical state *a* in Fig. 8) is a rare occurrence. Instead, it likely samples many iso-energetic, low-activity conformations with low energy barriers between them, and without a firm domain M anchor onto the membrane, the barrier for acquisition of the fully active conformation is large. In the solved structure of CCT-236, the αE_C and J segment are present, but not visible, indicating their disorder. Substituting Gly, Thr, or Ala for Tyr-213 slightly increases the fraction of the conformational ensemble with high activity (*e.g.* state a) at the expense of the unbent αE helix conformation (Fig. 8). For full-length CCT (or CCT-312) bound to the membrane via domain M, the conformational ensemble for the αE and J segment would be restricted, with a high proportion of fully active conformers (Fig. 8, state III). The folded M domain helix would provide an anchor point at the C terminus of the αE_C/J. The sequestered, compact environment for the αE hinge and the J segment suggested by the data in this paper and the companion paper (33) supports a constrained conformational ensemble in CCT_{mem}.

The αE helix residues Tyr-213 and Tyr-216 sample a solvent-protected environment in CCT_{mem}

Upon membrane binding, the AI helices dissociate from the αE helices, and thus the tyrosines of the αE hinge should become more solvent-accessible. However, iodination and fluorescence analysis showed that the new environment for these tyrosines in CCT_{mem} is not compatible with full solvent exposure. Previous work showing protection of Tyr-213 from chymotrypsin cleavage in CCT_{mem} (13) is in agreement with the protected status observed in the iodination experiments. The different iodination levels for Tyr-213 suggested different environments in the silenced, desilenced, and activated CCT forms, and this supports the modular conformational ensemble model for the allosteric linker. The Y216W substitution we made to probe fluorescence is nondisrupting, as it has no effect on the tertiary structure, membrane binding, or enzyme activity. Trp-216 was much less accessible to acrylamide in CCT_{mem} *versus* CCT_{sol}. The large increase in fluorescence intensity of Trp-216 upon membrane introduction also supports sequestration from solvent. However, Tyr-216 retained similar exposure to the I^+ species. Because the vesicle surface in the iodination reactions possessed very high negative charge (100% PG), the I^+ species would concentrate near the surface (<20 Å), and this is a potential weakness of the iodination analysis. Thus, the degree of protection indicated by the iodination levels for the αE tyrosines in CCT_{mem} could in fact be underestimated.

In CCT_{sol}, Trp-216 may be quenched by surrounding amino acids and is dequenched upon membrane binding. In the solved structure (PDB code 4MVC), Tyr-216 is situated within

quenching distance of Asn-220 and Tyr-213 in the αE and Met-292 in the AI. The dequenching and blue shift as well as the strong protection from acrylamide quenching observed for Trp-216 in CCT_{mem} is consistent with remodeling of the αE so that Trp-216 is in a chemically different and sequestered environment. That Tyr-216 can be substituted with Trp or Phe without functional consequences, but not with alanine (or cysteine)[6] also argues that the activated conformation places this residue in a nonpolar environment, and this is essential for activity.

An aromatic cluster between the two tyrosines in the αE and Phe-124 in L2 was observed as a dominant interaction *in silico* in all ten 1000-ns simulations lacking the AI helix (18). However, the aromatic clustering may not reflect the dominant conformers in CCT_{mem} *in vitro*. The simulated starting structures lacked the J segment, domain M, and a bilayer, and in their absence, the intrinsic drive to bury nonpolar residues resulted in the aromatic cluster. *In vitro* and *in vivo*, a bent helix may be stabilized by interactions other than or in addition to the aromatic cluster. Possibilities, explored in the companion paper (33), include interactions with the J segment following the αE and/or the membrane surface.

Our analysis of this previously unexplored, interdomain linker elucidates the αE_C/J segment as a signal transducer that has been evolutionarily tuned to elicit a response to membrane binding. The response includes hinge-induced reorientations, changes in solvent exposure, and new interactions forged by highly conserved residues. Data in the subsequent paper (33) suggest that the αE_C and J segments are close to the membrane surface in CCT_{mem} but are not membrane-penetrant and that they form a compact structure that brings the active site close to the membrane surface.

Experimental procedures

Materials

Pfu DNA polymerase, 10× polymerase buffer/$MgSO_4$, and DpnI restriction enzyme were from Thermo Fisher. dNTPs and SYPRO Orange dye (5000×) were from Invitrogen. Primers were from Integrated DNA Technologies. TOP10 and Rosetta competent *Escherichia coli* cells were originally from Novagen. Ampicillin, chloramphenicol, kanamycin, CTP, CDP-choline, pancreatic trypsin, phenylmethylsulfonyl fluoride, DTT, protease inhibitors, and imidazole were from Sigma. [^{14}C-Me]Phosphocholine was from PerkinElmer Life Sciences. Kanamycin, DTT, and isopropyl 1-thio-β-D-galactopyranoside were from Bioshop. Dialysis tubing was from Spectrum LifeSciences (molecular mass cutoff 12,000–14,000 kDa). Ni-NTA–agarose beads were from Qiagen. All phospholipids (POPC, egg PG, Br-PC 6,7/9,10/11,12, and dansyl-PE) were from Avanti Polar Lipids. Iodination Beads were from Pierce. ZipTips were from Millipore.

Construction, expression, and purification of CCTs

The untagged full-length rat CCTα was expressed in *Trichoplusia ni* cells using baculovirus infection and purified as described (12). The untagged catalytic fragment (CCTα-236) was also expressed and purified from *T. ni* cells (24). Construction of the N-terminally His-tagged, C-terminal truncations of rat CCTα were also described previously (15, 34). The truncated variants encoded CCTs terminating at residues 312, 304, 293, 271, 255, and 236. In addition to these, we used QuikChange mutagenesis (Stratagene) and HisCCT-236 as the template to construct HisCCT-212 by engineering a stop codon after codon 212.

We found during the progress of this work that engineering a C-terminal His tag increased the purity of the CCT-312 preparations fractionated on nickel-agarose. Thus, some of the constructs utilized a CCT-312 (His) variant (described previously (18)) as template for further mutagenesis. For spectroscopy in the presence of lipid vesicles, we found that deleting the N-terminal NLS sequence (^{12}RKRRK^{16}) eliminated turbidity of the samples caused by NLS-mediated vesicle aggregation (18, 34). Thus, all constructs to be used in fluorescence analysis utilized CCT-312-His Δ12–16 as template for further mutagenesis. Construct DNA sequences were analyzed by Eurofins Genomics, which confirmed the presence of the engineered mutation as well as the absence of any nonsolicited mutations. His tags for purification at either the N or C termini were provided by pET14b or pET24a plasmids, respectively. Tagged CCTs contained either the N-terminal, non-CCT sequence ($MGSSH_6SSGLVPRGSH$) or a C-terminal sequence following residue 312 (^{313}LEHHHHHH^{320}). Neither was cleaved prior to analysis. A list of the constructs, parent plasmids, and cell fractions for purification is provided in Table S1.

All constructs were expressed in *E. coli* Rosetta DE-3 cells (15). For cells harboring pET14b plasmids, the lysogeny broth growth medium contained 100 μg/ml ampicillin and 34 μg/ml chloramphenicol. For pET24a plasmids, the medium contained 50 μg/ml kanamycin and 34 μg/ml chloramphenicol. 400-ml cultures were agitated (225 rpm) at 37 °C until the optical density at 600 nm reached 0.45–0.55. CCT expression was induced with isopropyl β-D-1-thiogalactopyranoside (1 mM), and cultures were agitated for an additional 3 h at 37 °C (for CCT-312-His) or 20–21 °C (for His-CCT-236). After expression, cells were harvested by centrifugation at 4500 × *g* for 15 min and frozen at −80 °C. A small-scale analysis of CCT distribution between 20,000 × *g* supernatant and pellet fractions was done using a modification of a previously published procedure (5) to assess the appropriate fraction for purification.

Depending on partitioning behavior, the CCTs were purified from the soluble fraction, the particulate fraction, or the whole-cell lysate (see Table S1 for construct-specific information). Cell lysis and purification from the 20,000 × *g* supernatant by Ni-agarose chromatography was carried out as described (34, 35). To purify CCT from the 20,000 × *g* pellet, we washed the pellet twice using gentle sonication with lysis buffer (20 mM NaP_i, 150 mM NaCl, 1% Triton X-100, 2 mM DTT, protease inhibitors, pH 7.4), and the washed pellet was solubilized in 10 ml of denaturation buffer (6 M guanidinium-HCl, 500 mM NaCl, 50 mM NaP_i, pH 8, 25 mM imidazole, 1 mM DTT) by intermittent vortexing at 20–21 °C for 1 h. After removing nonsolubilized material by centrifugation for 20 min at 13,000 × *g* at 20–21 °C, the supernatant was applied to a 3–5-ml Ni-NTA–agarose column at 20–21 °C. The CCT was refolded on-col-

[6] S. G. Taneva, unpublished observation.

umn by successive washes with 20 ml of denaturation buffer containing 6, 5, 4, 3, 2, 1, and 0 M urea. CCT was eluted with 10 mM Tris, pH 8, 200 mM NaCl, 350 mM imidazole, 2 mM DTT. 1-ml elution fractions were dialyzed for 3 h against 10 mM Tris, pH 7.4, 0.2 M NaCl, 2 mM DTT. The dialyzed samples were centrifuged for 10 min at 13,000 × *g*, the supernatants were analyzed by SDS-PAGE, and the CCT-rich fractions were pooled and stored at −80 °C.

Some of the constructs were distributed between the soluble and particulate fractions. We found that CCT purification directly from the whole-cell lysate provided better yield without loss of purity for these CCTs. Cell pellets from 200-ml cultures were resuspended in 5 ml of lysis buffer with sonication on ice. The lysate (5 ml) was added to 50 ml of 50 mM NaP_i, pH 8, 6 M guanidinium HCl, 500 mM NaCl, 25 mM imidazole, 1% Triton X-100, 1 mM DTT, gently mixed for 1 h at 20–21 °C, and centrifuged at 13,000 × *g* for 30 min. The supernatant was applied to a Ni-NTA–agarose column at 20–21 °C, and the CCT was isolated as described above. The concentrations of the pure enzymes were determined by the method of Bradford (36) using BSA as a standard.

CCT enzyme activity

The specific activity was determined as described previously (5). For the standard assay, optimal for WT CCT, the concentrations of CTP and phosphocholine in the assay were 8 and 1.6 mM, respectively. Kinetic constants were determined by varying the CTP concentration from 0 to 16 mM using a fixed (2 mM) concentration of phosphocholine. The data were evaluated with GraphPad Prism, and the V_{max} and K_m values were obtained using this software. r^2 values for the fits to the data were >0.96. Sonicated lipid vesicles were prepared as described previously (37), except the suspensions were sonicated for 15 min on 50% output and were centrifuged for 4 min at 13,000 × *g* to remove titanium debris introduced by the sonicator probe. The vesicles were stored under argon at 4 °C and used within ~2 days.

Thermal denaturation using SYPRO Orange

The T_m for unfolding was measured using the hydrophobic dye SYPRO Orange (Invitrogen, Molecular Probes), as described (5).

Iodination of CCTs

Iodination of untagged CCT-236 and full-length CCT-367 utilized chloramine-T–derivatized Iodination Beads. A single bead washed in 10 mM Tris, pH 6.5, was placed into a microcentrifuge tube together with 100 μl of 3.5 mM NaI, 10 mM Tris, pH 6.5, and incubated for 5 min. The Iodination Bead was removed, and aliquots from the reaction solution containing the oxidized I^+ were added to 0.1-ml samples containing 20 μM protein in 10 mM Tris, pH 7.4, 100 mM NaCl, 0.2 mM DTT to give a final molar ratio of NaI to tyrosine of 0, 1, 2, 3, and 5. The resulting mixtures were incubated for 2 min (or 4 min for NaI/tyrosine = 5) at 20–21 °C, and the reaction was stopped by the addition of DTT to a final concentration of 3 mM. Aliquots were removed to assess the completeness of iodination based on a detectable mass shift via SDS-PAGE analysis. The remainder was digested with trypsin for 1 h at 37 °C using a trypsin/CCT mass ratio of 0.2. The digestion was quenched with 2 mM phenylmethylsulfonyl fluoride.

Iodination of membrane-bound CCT was performed as above in the presence of a 100-fold molar excess of PG sucrose-loaded vesicles (SLVs). SLVs were prepared by extrusion of multilamellar vesicles at 20–21 °C using polycarbonate membranes with a 100-nm pore diameter (38). The protein-SLV mixtures were incubated for 5 min at 20–21 °C. After iodination and trypsin digestion as described above, the SLVs were sedimented at 100,000 × *g* for 1 h at 20 °C to remove lipid. The supernatant was removed and used for MS analysis.

For MS analysis, we adjusted the pH of the protein digest to pH ≤4.0 with TFA (final concentration of 0.1%). We desalted 25-μl samples using 0.6 μl of $ZipTip_{C18}$ resin according to the manufacturer's protocol (Millipore). Peptides were eluted from the ZipTip with 10 μl of 50% acetonitrile, 0.1% TFA.

HPLC-MS analysis of iodinated CCT peptides

Iodinated and desalted protein digests were analyzed with a Bruker maXis Impact Quadrupole Time-of-Flight LC/MS System. The system consists of an Agilent 1200 HPLC and a Bruker maXis Impact Ultra-High Resolution tandem TOF mass spectrometer. We used positive electrospray ionization for MS and MS/MS experiments and the following parameters: gas temperature at 180 °C, gas flow rate at 9 liters/min, nebulizer at 4 bars, capillary voltage at 3800 or 4200 V, analyte mass range of 50–1500 Da, and mass-dependent collision energies ranging from 10 to 40 eV. Data acquisition and processing utilized Compass 1.5 and Biotools 3.2 SR3 software provided by the Bruker system.

We used two different HPLC separation methods, which are briefly summarized here. Details of these methods are described in the supporting material. 1) "Fast" LC/MS was used to determine the extent of iodination of all of the tyrosine-containing peptides in CCT_{sol} and CCT_{mem}. We obtained the peak intensities for the tyrosine-containing peptides that matched the theoretical masses in a list of CCT peptides containing 0, 1, or 2 iodines (or 3 or 4 iodines in the case of peptides containing 2 tyrosines). The extent of tyrosine iodination was determined as the ratio of the peak intensity of the modified peptide to the sum of the intensities of modified and unmodified peptides. The data from this method appear in Table 2 and Fig. S4. 2) "Slow" LC/MS was used to resolve the isomers of the αE heptapeptides containing all of the iodinated species of Tyr-213 and Tyr-216, coupled to MS/MS fragmentation to identify the iodinated tyrosines in each resolved species. The relative abundance of the various iodinated species of this αE peptide was assessed from extracted ion chromatograms that segregated the *m*/*z* species matched to each iodinated and unmodified peptide away from all other CCT peptides (Fig. S5). Quantitative analysis utilized integrated peak areas from these chromatograms. The two mono-iodinated species (^{212}D**Y**(I)DVYAR^{218} and ^{212}DYDV**Y**(I)AR^{218}) did not separate by the first two methods. Their relative abundance was obtained from fragmentation analysis. The data using the latter methods appear in Fig. 6.

Tryptophan fluorescence and acrylamide quenching

For fluorescence acquisition, 3 μM CCT was incubated in buffer (10 mM Tris, pH 7.4, 150 mM NaCl, 2 mM DTT) or 450 μM vesicles in buffer for 5 min at 20–21 °C. Sonicated POPC/egg PG (1:1) vesicles (2 mM lipid) were prepared as described above. Sample volume was 0.3 ml. Fluorescence scans were measured at 20 °C on a Cary Eclipse fluorescence spectrophotometer. The excitation wavelength was 295 nm (to minimize tyrosine excitation) with a 5-nm excitation slit, and the emission was scanned twice from 305 to 420 nm with a 10-nm emission slit and a scan rate of 120 nm/min. Acrylamide (6 μmol) was added to the same sample with pipette-mixing to a final concentration of 20 mM, and the fluorescence scan was repeated. This cycle was continued in 20 mM increments to a final acrylamide concentration of 120 mM. Lipid and spent dialysis buffer background spectra were subtracted to generate corrected emission spectra. The fluorescence intensity maximum for each spectrum was recorded at the peak emission wavelength average for each acrylamide quenching set, and these values were used to generate linear plots of unquenched/quenched fluorescence *versus* concentration of acrylamide for each single-Trp CCT construct. The slopes of these plots were reported as the Stern–Volmer quenching constants (K_{SV}) in the absence and presence of vesicles,

$$F_o/F_q = K_{sv}([Q]) + 1 \quad \text{(Eq. 1)}$$

where F_o represents unquenched fluorescence, F_q is quenched fluorescence, and $[Q]$ is the molar concentration of acrylamide.

Author contributions—S. G. T., J. L., D. G. K., and R. B. C. conceptualization; S. G. T., D. G. K., and R. B. C. data curation; S. G. T., D. G. K., H. C., and R. B. C. formal analysis; S. G. T. and R. B. C. validation; S. G. T., J. L., D. G. K., C. T., H. C., and R. B. C. investigation; S. G. T., D. G. K., H. C., and R. B. C. visualization; S. G. T., J. L., D. G. K., H. C., and R. B. C. methodology; S. G. T., J. L., D. G. K., C. T., H. C., and R. B. C. writing-review and editing; J. L. and R. B. C. supervision; R. B. C. funding acquisition; R. B. C. writing-original draft; R. B. C. project administration.

Acknowledgments—We thank Dr. Peter Tieleman for valuable comments on the manuscript and Ronnie Tse for his contribution early in the project.

References

1. Cornell, R. B., and Ridgway, N. D. (2015) CTP:phosphocholine cytidylyltransferase: function, regulation, and structure of an amphitropic enzyme required for membrane biogenesis. *Prog. Lipid Res.* **59,** 147–171 CrossRef Medline
2. Ding, Z., Taneva, S. G., Huang, H. K., Campbell, S. A., Semenec, L., Chen, N., and Cornell, R. B. (2012) A 22-mer segment in the structurally pliable regulatory domain of metazoan CTP:phosphocholine cytidylyltransferase facilitates both silencing and activating functions. *J. Biol. Chem.* **287,** 38980–38991 CrossRef Medline
3. Yang, W., Boggs, K. P., and Jackowski, S. (1995) The association of lipid activators with the amphipathic helical domain of CTP:phosphocholine cytidylyltransferase accelerates catalysis by increasing the affinity of the enzyme for CTP. *J. Biol. Chem.* **270,** 23951–23957 CrossRef Medline
4. Cornell, R. B. (2016) Membrane lipid compositional sensing by the inducible amphipathic helix of CCT. *Biochim. Biophys. Acta* **1861,** 847–861 CrossRef Medline
5. Cornell, R. B., Taneva, S. G., Dennis, M. K., Tse, R., Dhillon, R. K., and Lee, J. (2019) Disease-linked mutations in the phosphatidylcholine regulatory enzyme CCTα impair enzymatic activity and fold stability. *J. Biol. Chem.* **294,** 1490–1501 CrossRef Medline
6. Hoover-Fong, J., Sobreira, N., Jurgens, J., Modaff, P., Blout, C., Moser, A., Kim, O. H., Cho, T. J., Cho, S. Y., Kim, S. J., Jin, D. K., Kitoh, H., Park, W. Y., Ling, H., Hetrick, K. N., *et al.* (2014) Mutations in PCYT1A, encoding a key regulator of phosphatidylcholine metabolism, cause spondylometaphyseal dysplasia with cone-rod dystrophy. *Am. J. Hum. Genet.* **94,** 105–112 CrossRef Medline
7. Payne, F., Lim, K., Girousse, A., Brown, R. J., Kory, N., Robbins, A., Xue, Y., Sleigh, A., Cochran, E., Adams, C., Dev Borman, A., Russel-Jones, D., Gorden, P., Semple, R. K., Saudek, V., O'Rahilly, S., Walther, T. C., Barroso, I., and Savage, D. B. (2014) Mutations disrupting the Kennedy phosphatidylcholine pathway in humans with congenital lipodystrophy and fatty liver disease. *Proc. Natl. Acad. Sci. U.S.A.* **111,** 8901–8906 CrossRef Medline
8. Testa, F., Filippelli, M., Brunetti-Pierri, R., Di Fruscio, G., Di Iorio, V., Pizzo, M., Torella, A., Barillari, M. R., Nigro, V., Brunetti-Pierri, N., Simonelli, F., and Banfi, S. (2017) Mutations in the PCYT1A gene are responsible for isolated forms of retinal dystrophy. *Eur. J. Hum. Genet.* **25,** 651–655 CrossRef Medline
9. Yamamoto, G. L., Baratela, W. A., Almeida, T. F., Lazar, M., Afonso, C. L., Oyamada, M. K., Suzuki, L., Oliveira, L. A., Ramos, E. S., Kim, C. A., Passos-Bueno, M. R., and Bertola, D. R. (2014) Mutations in PCYT1A cause spondylometaphyseal dysplasia with cone-rod dystrophy. *Am. J. Hum. Genet.* **94,** 113–119 CrossRef Medline
10. Arnold, R. S., and Cornell, R. B. (1996) Lipid regulation of CTP:phosphocholine cytidylyltransferase: electrostatic, hydrophobic, and synergistic interactions of anionic phospholipids and diacylglycerol. *Biochemistry* **35,** 9917–9924 CrossRef Medline
11. Johnson, J. E., Rao, N. M., Hui, S. W., and Cornell, R. B. (1998) Conformation and lipid binding properties of four peptides derived from the membrane-binding domain of CTP:phosphocholine cytidylyltransferase. *Biochemistry* **37,** 9509–9519 CrossRef Medline
12. Taneva, S., Johnson, J. E., and Cornell, R. B. (2003) Lipid-induced conformational switch in the membrane binding domain of CTP:phosphocholine cytidylyltransferase: a circular dichroism study. *Biochemistry* **42,** 11768–11776 CrossRef Medline
13. Bogan, M. J., Agnes, G. R., Pio, F., and Cornell, R. B. (2005) Interdomain and membrane interactions of CTP:phosphocholine cytidylyltransferase revealed via limited proteolysis and mass spectrometry. *J. Biol. Chem.* **280,** 19613–19624 CrossRef Medline
14. Huang, H. K., Taneva, S. G., Lee, J., Silva, L. P., Schriemer, D. C., and Cornell, R. B. (2013) The membrane-binding domain of an amphitropic enzyme suppresses catalysis by contact with an amphipathic helix flanking its active site. *J. Mol. Biol.* **425,** 1546–1564 CrossRef Medline
15. Lee, J., Taneva, S. G., Holland, B. W., Tieleman, D. P., and Cornell, R. B. (2014) Structural basis for autoinhibition of CTP: phosphocholine cytidylyltransferase (CCT), the regulatory enzyme in phosphatidylcholine synthesis, by its membrane-binding amphipathic helix. *J. Biol. Chem.* **289,** 1742–1755 CrossRef Medline
16. Guca, E., Nagy, G. N., Hajdú, F., Marton, L., Izrael, R., Hoh, F., Yang, Y., Vial, H., Vértessy, B. G., Guichou, J.-F., and Cerdan, R. (2018) Structural determinants of the catalytic mechanism of Plasmodium CCT, a key enzyme of malaria lipid biosynthesis. *Sci. Rep.* **8,** 11215 CrossRef Medline
17. Helmink, B. A., Braker, J. D., Kent, C., and Friesen, J. A. (2003) Identification of lysine 122 and arginine 196 as important functional residues of rat CTP:phosphocholine cytidylyltransferase α. *Biochemistry* **42,** 5043–5051 CrossRef Medline
18. Ramezanpour, M., Lee, J., Taneva, S. G., Tieleman, D. P., and Cornell, R. B. (2018) An auto-inhibitory helix in CTP:phosphocholine cytidylyltransferase hijacks the catalytic residue and constrains a pliable, domain-bridging helix pair. *J. Biol. Chem.* **293,** 7070–7084 CrossRef Medline
19. Lee, J., Johnson, J., Ding, Z., Paetzel, M., and Cornell, R. B. (2009) Crystal structure of a mammalian CTP:phosphocholine cytidylyltransferase catalytic domain reveals novel active site residues within a highly conserved

nucleotidyltransferase fold. *J. Biol. Chem.* **284,** 33535–33548 CrossRef Medline
20. Park, Y. S., Gee, P., Sanker, S., Schurter, E. J., Zuiderweg, E. R., and Kent, C. (1997) Identification of functional conserved residues of CTP:glycerol-3-phosphate cytidylyltransferase: role of histidines in the conserved HXGH in catalysis. *J. Biol. Chem.* **272,** 15161–15166 CrossRef Medline
21. Pattridge, K. A., Weber, C. H., Friesen, J. A., Sanker, S., and Kent, C., and Ludwig, M. L. (2003) Glycerol-3-phosphate cytidylyltransferase: structural shanges induced by binding of CDP-glycerol and the role of lysine residues in catalysis. *J. Biol. Chem.* **278,** 51863–51871 CrossRef Medline
22. Weber, C. H., Park, Y. S., Sanker, S., Kent, C., and Ludwig, M. L. (1999) A prototypical cytidylyltransferase: CTP:glycerol-3-phosphate cytidylyltransferase from *Bacillus subtilis*. *Structure* **7,** 1113–1124 CrossRef Medline
23. Dennis, M. K., Taneva, S. G., and Cornell, R. B. (2011) The intrinsically disordered nuclear localization signal and phosphorylation segments distinguish the membrane affinity of two cytidylyltransferase isoforms. *J. Biol. Chem.* **286,** 12349–12360 CrossRef Medline
24. Friesen, J. A., Campbell, H. A., and Kent, C. (1999) Enzymatic and cellular characterization of a catalytic fragment of CTP:phosphocholine cytidylyltransferase α. *J. Biol. Chem.* **274,** 13384–13389 CrossRef Medline
25. Wang, Y., and Kent, C. (1995) Identification of an inhibitory domain of CTP:phosphocholine cytidylyltransferase. *J. Biol. Chem.* **270,** 18948–18952 CrossRef Medline
26. Cornell, R. B., Kalmar, G. B., Kay, R. J., Johnson, M. A., Sanghera, J. S., and Pelech, S. L. (1995) Functions of the C-terminal domain of CTP:phosphocholine cytidylyltransferase: effects of C-terminal deletions on enzyme activity, intracellular localization and phosphorylation potential. *Biochem. J.* **310**, 699–708 CrossRef Medline
27. Yang, W., and Jackowski, S. (1995) Lipid activation of CTP:phosphocholine cytidylyltransferase is regulated by the phosphorylated carboxyl-terminal domain. *J. Biol. Chem.* **270,** 16503–16506 CrossRef Medline
28. Lykidis, A., Jackson, P., and Jackowski, S. (2001) Lipid activation of CTP:phosphocholine cytidylyltransferase alpha: characterization and identification of a second activation domain. *Biochemistry* **40,** 494–503 CrossRef Medline
29. Arnold, R. S., DePaoli-Roach, A. A., and Cornell, R. B. (1997) Binding of CTP:phosphocholine cytidylyltransferase to lipid vesicles: diacylglycerol and enzyme dephosphorylation increase the affinity for negatively charged membranes. *Biochemistry* **36,** 6149–6156 CrossRef Medline
30. Chong, S. S., Taneva, S. G., Lee, J. M., and Cornell, R. B. (2014) The curvature sensitivity of a membrane-binding amphipathic helix can be modulated by the charge on a flanking region. *Biochemistry* **53,** 450–461 CrossRef Medline
31. Johnson, J. E., and Cornell, R. B. (1994) Membrane-binding amphipathic α-helical peptide derived from CTP:phosphocholine cytidylyltransferase. *Biochemistry* **33,** 4327–4335 CrossRef Medline
32. Johnson, J. E., Xie, M., Singh, L. M., Edge, R., and Cornell, R. B. (2003) Both acidic and basic amino acids in an amphitropic enzyme, CTP:phosphocholine cytidylyltransferase, dictate its selectivity for anionic membranes. *J. Biol. Chem.* **278,** 514–522 CrossRef Medline
33. Knowles, D. G., Lee, J., Taneva, S. G., and Cornell, R. B. (2019) Remodelling of the allosteric linker upon membrane binding of CCTα pulls its active site close to the membrane surface. *J. Biol. Chem.* **294,** jbc.RA119.009850 CrossRef Medline
34. Taneva, S., Dennis, M. K., Ding, Z., Smith, J. L., and Cornell, R. B. (2008) Contribution of each membrane binding domain of the CTP:phosphocholine cytidylyltransferase-α dimer to its activation, membrane binding, and membrane cross-bridging. *J. Biol. Chem.* **283,** 28137–28148 CrossRef Medline
35. Xie, M., Smith, J. L., Ding, Z., Zhang, D., and Cornell, R. B. (2004) Membrane binding modulates the quaternary structure of CTP:phosphocholine cytidylyltransferase. *J. Biol. Chem.* **279,** 28817–28825 CrossRef Medline
36. Bradford, M. M. (1976) A rapid and sensitive method for the quantitation of microgram quantities of protein utilizing the principle of protein-dye binding. *Anal. Biochem.* **72,** 248–254 CrossRef Medline
37. Sohal, P. S., and Cornell, R. B. (1990) Sphingosine inhibits the activity of rat liver CTP:phosphocholine cytidylyltransferase. *J. Biol. Chem.* **265,** 11746–11750 Medline
38. Taneva, S. G., Patty, P. J., Frisken, B. J., and Cornell, R. B. (2005) CTP:phosphocholine cytidylyl-transferase binds anionic phospholipid vesicles in a cross-bridging mode. *Biochemistry* **44,** 9382–9393 CrossRef Medline